Control of Multiagent Systems with Local and Global Objectives: Experimental Results

Emre Yildirim*, Selahattin Burak Sarsilmaz†, Dzung Tran‡, and Tansel Yucelen§

University of South Florida

We focus on multiagent systems that have capabilities to accomplish global and local objectives. The former refers to a task (e.g., reaching a consensus, following a leader and so on), which is expected to be performed eventually by all agents in the system, and the latter is a kind of the secondary objective of the multiagent system, which is desired to be achived by only a certain number of agents without deteriorating the global objective of the multiagent system. To this end, the authors of [1] proposed five different distributed protocols having comparable advantages with system-theoretic stability analyses for multiagent systems being subject to a global objective, which is a leaderless consensus, and local objectives. In addition, we slightly modify these protocols in order to achieve the leader-follower consensus as a global objective. The contribution of this paper is to conduct experiments on a team of ground mobile robots with the protocols mentioned above and to make comparisons of their performances.

I Introduction

Multiagent systems consist of agents that exchange and process distributed information with respect to a graph topology. Since multiagent systems have been an active research topic in the control systems community over the last two decades, major issues (e.g., consensus, formation, and so on) have been addressed in numerous studies (e.g., see [2] and [3]). Despite all the developments in multiagent systems literature, the authors of [1] have recently raised the following question: *How do several agents forming the multiagent system perform their own local objectives without deteriorating the overall multiagent system's global objective?*. Here, local objectives refer to tasks (e.g., sending some agents to desired points for various purposes such as data collection, battery recharging, and so on) assigned to certain agents and the global objective refers to a task (e.g., leaderless consensus, leader-follower consensus, formation, containment and so on), which is desired to be achieved eventually by all agents in the multiagent system. This question was addressed in [1] by providing five different distributed protocols with comparable advantages (see Tables 1 and 2 in [1]) for single integrator agents with system-theoretic stability analyses.

In this paper, we provide an experimental study of implementing five leaderless consensus protocols (LCPs) in [1] and five leader-follower consensus protocols (L-FCPs) on a team of ground mobile robots (see

* Emre Yildirim is a Graduate Student of the Department of Mechanical Engineering and a Member of the Laboratory for Autonomy, Control, Information, and Systems (LACIS, http://lacis.eng.usf.edu/) at the University of South Florida, Tampa, FL 33620, USA (email: emreyildirim@mail.usf.edu). He is also the Recipient of the Republic of Turkey Ministry of National Education Scholarship.

† Selahattin Burak Sarsilmaz is a Graduate Research Assistant of the Department of Mechanical Engineering and a Member of the Laboratory for Autonomy, Control, Information, and Systems (LACIS, http://lacis.eng.usf.edu/) at the University of South Florida, Tampa, FL 33620, USA (email: sarsilmaz@mail.usf.edu).

‡ Dzung Tran is a Graduate Research Assistant of the Department of Mechanical Engineering and a Member of the Laboratory for Autonomy, Control, Information, and Systems (LACIS, http://lacis.eng.usf.edu/) at the University of South Florida, Tampa, FL 33620, USA (email: dtran3@mail.usf.edu).

§ Tansel Yucelen is an Assistant Professor of the Department of Mechanical Engineering and the Director of the Laboratory for Autonomy, Control, Information, and Systems (LACIS, http://lacis.eng.usf.edu/) at the University of South Florida, Tampa, FL 33620, USA (email: yucelen@usf.edu). T. Yucelen is also a Senior Member of the American Institute of Aeronautics and Astronautics and a Member of the National Academy of Inventors.

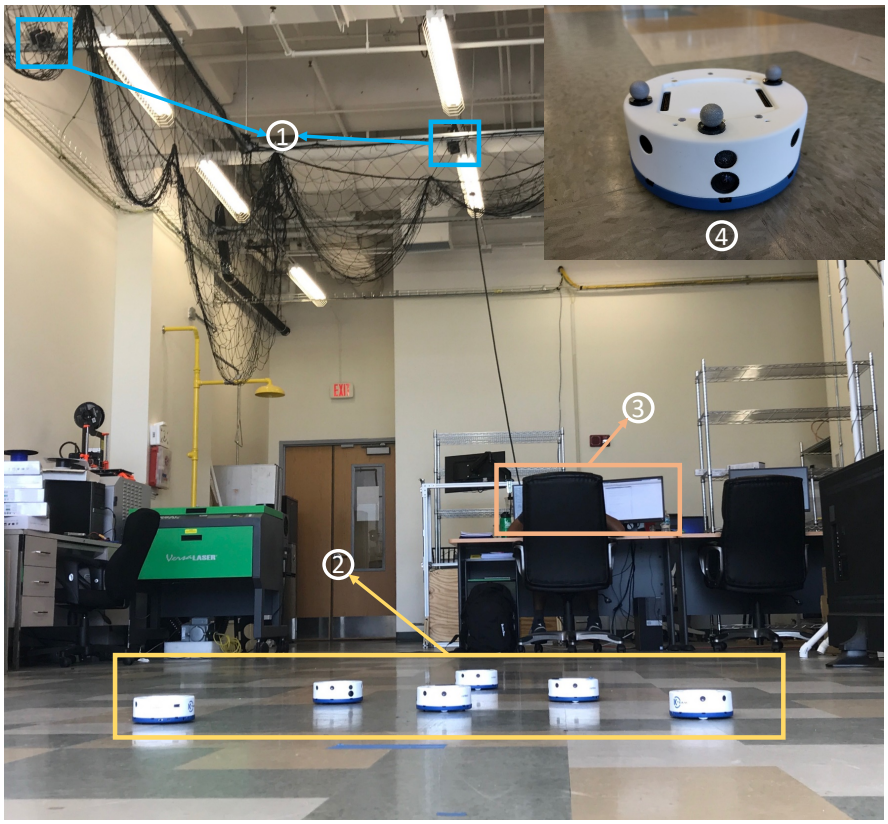

Figure 1. The experimental setup with 1) the motion capture cameras, 2) a group of Khepera IV ground mobile robots, 3) the workstation computer, and 4) the closer view of a Khepera IV ground mobile robot.

Figure 1) to compare the performance of all protocols. We first summarize the important aspects of the former protocols and present the latter protocols in Section III. With regard to the experimental setup, we utilize the motion capture camera system mounted at the top of the workspace of the robots, six Khepera IV ground mobile robots, and the workstation for information exchange between the camera system and each robot. In our experiment, local and global objectives are clearly defined in Section IV, where the former is assigned to a certain number of the robots with the expectation of achieving the latter eventually. In addition, the rest of robots accomplish only the latter during the whole experiment.

II Mathematical Preliminaries

In this paper, we follow the same notation presented in [1]. To be self-contained, the set of real and positive real numbers are denoted by $\mathbb{R}$ and $\mathbb{R}_{>0}$, respectively. The set of $n \times 1$ real column vectors is denoted by $\mathbb{R}^n$, the set of $n \times m$ real matrices is denoted by $\mathbb{R}^{n\times m}$, and $n \times 1$ vector of all ones is denoted by $\mathbf{1}_n$. Finally, "$\triangleq$" denotes equality by definition and $\text{diag}(a_1, \ldots, a_n)$ denotes a diagonal matrix with scalar entries $a_1, \ldots, a_n$ on its diagonal.

Now, we highlight graph theoretical notations adopted in [1]. Consider a fixed (i.e., time-invariant) directed graph $\mathcal{G} = (V, E)$ with $V = \{v_1, ..., v_N\}$ being a nonempty finite set of N nodes and $E \subset V \times V$ being a set of edges. In particular, each node in V corresponds to an agent (i.e., robot). There is an edge rooted at node v_j and ended at v_i, (i.e., $(v_j, v_i) \in E$), if and only if v_i receives information from v_j. $A = [a_{ij}] \in \mathbb{R}^{N\times N}$ denotes the adjacency matrix of the graph $\mathcal{G}$, where $a_{ij} > 0$ if $(v_j, v_i) \in E$, $a_{ij} = 0$ otherwise. Self loops are not allowed (i.e., $a_{ii} = 0, \forall i \in \mathcal{N}$, where $\mathcal{N} = \{1, ..., N\}$). In addition, N_i denotes the set of neighbors of node v_i such that $N_i = \{j \in V | (v_j, v_i) \in E\}$. We define in-degree matrix and Laplacian matrices of the graph $\mathcal{G}$ as $D = \text{diag}(d_1, ..., d_N)$ with $d_i = \sum_{j\in N_i} a_{ij}$ and $L = D - A$, respectively. Moreover, a directed path

starting from v_i ending at v_j is a sequence of successive edges in the form $\{(v_i, v_p), (v_p, v_q), \ldots, (v_r, v_j)\}$. A directed graph is said to have a spanning tree if there is a root node such that it has a directed path to every other node in the graph. A fixed augmented directed graph is defined as $\bar{\mathcal{G}} = (\bar{V}, \bar{E})$, where $\bar{V} = V \cup \{v_0\}$ is the set of $N+1$ nodes, including all nodes in V and the leader node v_0, and $\bar{E} = E \cup E'$ is the set of edges with E' being a proper subset of $\{(v_0, v_i) |\ i \in \mathcal{N}\}$.

III Problem Setup and Protocols: An Overview

We first concisely summarize the essential theoretical parts of [1], which only considers LCPs. Then, we introduce L-FCPs, which are obtained by slightly modifying LCPs in [1]. To begin with, we consider a multiagent system composed of N agents having single integrator dynamics over a fixed and directed graph $\mathcal{G}$. The dynamics of each agent is given by

$$\dot{x}_i(t) \quad = \quad u_i(t), \quad x_i(0) = x_{i0}, \quad t \geq 0, \tag{1}$$

with the state $x_i(t) \in \mathbb{R}$ and the input $u_i(t) \in \mathbb{R}$. Let us define $x(t) \triangleq [x_1(t), \ldots, x_N(t)]^{\mathrm{T}}$. Moreover, the multiagent system is assigned the task of achieving global and local objectives. In particular, the global objective refers to achieving a consensus by neighbor-based information exchange and the local objective is a task assigned to a subset of agents forming the multiagent system.

The set of agents that are (respectively, are not) assigned local tasks is denoted by $\mathcal{N}_{\mathrm{p}} \subset \mathcal{N}$ (respectively, $\mathcal{N}_{\mathrm{p}'} \subset \mathcal{N}$). Throughout this paper, we consider that the roles of agents are fixed. Clearly, $\mathcal{N} = \mathcal{N}_{\mathrm{p}} \cup \mathcal{N}_{\mathrm{p}'}$ and $\mathcal{N}_{\mathrm{p}} \cap \mathcal{N}_{\mathrm{p}'} = \emptyset$. Without loss of generality, we assume the index sets as $\mathcal{N}_{\mathrm{p}} = \{1, ..., p\}$ and $\mathcal{N}_{\mathrm{p}'} = \{p+1, ..., N\}$.

To address the problem stated in Section I, five different LCPs are given in [1], which takes the following properties into consideration:

i) Agents (i.e., $\mathcal{N}_{\mathrm{p}'}$) execute their global objective irrespective of the local objectives performed by other agents (i.e., $\mathcal{N}_{\mathrm{p}}$); in other words, $\lim_{t\to\infty}(x_i(t) - x^*) = 0, \forall i \in \mathcal{N}_{\mathrm{p}'}$, where $x^* \in \mathbb{R}$ is a consensus value.

ii) The global objective of the multiagent system is followed by agents (i.e., $\mathcal{N}_{\mathrm{p}}$), which accomplish their local tasks; in other words, $\lim_{t\to\infty}(x_i(t) - x^*) = 0, \forall i \in \mathcal{N}_{\mathrm{p}}$ if $\lim_{t\to\infty} \theta_i(t) = 0, \forall i \in \mathcal{N}_{\mathrm{p}}$, where $\theta_i(t) \in \mathbb{R}$ is a piecewise continuous input used to assign local tasks.

If we replace x^* in the properties *i*) and *ii*) with r, which is a constant external reference signal from the leader, then L-FCPs also take into account the above properties (see Remark 2). Before summarizing the protocols, we list the assumptions used in this paper:

Assumption 1. The directed graph $\mathcal{G}$ is fixed and has a spanning tree.

Assumption 2. Each agent $i \in \mathcal{N}_{\mathrm{p}}$ receives information from at least one agent $j \in \mathcal{N}_{\mathrm{p}'}$.

Assumption 3. For all $i \in \mathcal{N}_{\mathrm{p}'}$, one sets $x_{\mathrm{r}i0} = x_{i0}$.

Assumption 4. The directed graph $\bar{\mathcal{G}}$ has a spanning tree with the root node being the leader node.

Remark 1. We utilize Assumptions 1-3 for LCPs. However, we replace Assumption 1 with Assumption 4 in L-FCPs while retaining other assumptions. We also note that Assumptions 2 and 3 are not necessary to address the question stated in the introduction. In particular, Assumption 3 is required only for the first protocol of LCPs and L-FCPs, and Assumption 2 is not used by the fourth and fifth protocols of LCPs and L-FCPs. Let $d_{\mathrm{p}i} \triangleq \sum_{j\in N_i \setminus \mathcal{N}_{\mathrm{p}}} a_{ij}$ be another in-degree for each agent $i \in \mathcal{N}_{\mathrm{p}}$. As a result of Assumption 2, $d_{\mathrm{p}i} > 0$, $\forall i \in \mathcal{N}_{\mathrm{p}}$.

A Leaderless Consensus as a Global Objective

1 First Protocol (LCP 1)

We now summarize the first protocol given in [1], which utilizes the reference consensus model for each agent given by

$$\dot{x}_{\mathrm{r}i}(t) \quad = \quad \sum_{j\in N_i} a_{ij}(x_{\mathrm{r}j}(t) - x_{\mathrm{r}i}(t)), \quad x_{\mathrm{r}i}(0) = x_{\mathrm{r}i0}, \quad t \geq 0. \tag{2}$$

Let $x_{\mathrm{r}}(t) \triangleq [x_{\mathrm{r}1}(t), \dots x_{\mathrm{r}N}(t)] \in \mathbb{R}^N$. Then, the dynamics of all reference consensus models can be written as

$$\dot{x}_{\mathrm{r}}(t) \quad = \quad -Lx_{\mathrm{r}}, \quad x_{\mathrm{r}}(0) = x_{\mathrm{r}0}, \quad t \geq 0. \tag{3}$$

Then, the first protocol[a] is given by

$$u_i(t) \quad = \quad \sum_{j \in N_i} a_{ij}(x_{\mathrm{r}j}(t) - x_{\mathrm{r}i}(t)) + k_i\Big(\theta_i(t) + \sum_{j \in N_i \setminus \mathcal{N}_{\mathrm{p}}} a_{ij}\big(x_j(t) - x_i(t)\big)\Big), \tag{4}$$

where, $k_i \in \mathbb{R}_{>0}$ if $i \in \mathcal{N}_{\mathrm{p}}$, $k_i = 0$ otherwise. Note that (4) shows that each agent in the graph $\mathcal{G}$ is assumed to interchange the relative reference model states with respect to its neighboring agents. In addition, it is also assumed that each agent has access to $(x_j(t) - x_i(t))$ for all $j \in N_i \setminus \mathcal{N}_{\mathrm{p}}$. By the definition of k_i, the second summation in the right-hand side of (4) makes no contribution to agents belonging to $\mathcal{N}_{\mathrm{p}'}$.

2 Second Protocol (LCP 2)

In this protocol, the reference consensus model (2) is used for only agents in $\mathcal{N}_{\mathrm{p}}$, which removes the requirement of Assumption 3 and also reduces the order of the protocols for each agent $i \in \mathcal{N}_{\mathrm{p}'}$. Let $q(t) \triangleq [x_{\mathrm{r}1}(t), \dots, x_{\mathrm{r}p}(t), x_{p+1}(t), \dots, x_N(t)]^{\mathrm{T}} \in \mathbb{R}^N$, where the first p elements represent the state of reference consensus model of each agent $i \in \mathcal{N}_{\mathrm{p}}$ and the rest represents the state of each agent $i \in \mathcal{N}_{\mathrm{p}'}$. The reference consensus model for each agent $i \in \mathcal{N}_{\mathrm{p}}$ is given by

$$\dot{x}_{\mathrm{r}i}(t) = \sum_{j \in N_i} a_{ij}(q_j(t) - q_i(t)), \quad x_{\mathrm{r}i}(0) = x_{\mathrm{r}i0}, \quad t \geq 0. \tag{5}$$

Now, we can present the second protocol as

$$u_i(t) = \sum_{j \in N_i} a_{ij}(q_j(t) - q_i(t)) + k_i\Big(\theta_i(t) + \sum_{j \in N_i \setminus \mathcal{N}_{\mathrm{p}}} a_{ij}\big(x_j(t) - x_i(t)\big)\Big). \tag{6}$$

Inserting (6) into (2), the dynamics of each agent $i \in \mathcal{N}_{\mathrm{p}'}$ becomes

$$\dot{x}_i(t) = \sum_{j \in N_i} a_{ij}(q_j(t) - q_i(t)), \quad x_i(0) = x_0, \quad t \geq 0. \tag{7}$$

When we consider (5) and (7) together, we can write the aggregated dynamics as

$$\dot{q}(t) \quad = \quad -Lq, \quad q(0) = q_0, \quad t \geq 0. \tag{8}$$

In contrast to (4), additional information exchange is required in (6) since $\big(q_j(t) - q_i(t)\big)$ can denote $\big(x_{\mathrm{r}j}(t) - x_{\mathrm{r}i}(t)\big)$ or $\big(x_j(t) - x_{\mathrm{r}i}(t)\big)$ for agents in $\mathcal{N}_{\mathrm{p}}$ and $\big(x_{\mathrm{r}j}(t) - x_i(t)\big)$ or $\big(x_j(t) - x_i(t)\big)$ for agents in $\mathcal{N}_{\mathrm{p}'}$. Note that the desired consensus value can be selected by arranging the initial values of the reference consensus model of each agent $i \in \mathcal{N}$ in the first protocol. Due to the structure of $q(t)$, the second protocol does not provide the flexibility in selecting the desired consensus value in general.

3 Third Protocol (LCP 3)

Now, we present the third protocol, which provides not only a flexibility to select a desired consensus value but also a capability to achieve it as a global objective. This protocol is the same as the first protocol except

[a] All protocols in this paper consider k_i as defined in the first protocol.

a damping term inserted into each agent $i \in \mathcal{N}_{\mathrm{p}'}$. Then the third protocol has the form given by

$$u_i(t) \;=\; l_i(x_{\mathrm{r}i}(t) - x_i(t)) + \sum_{j\in N_i} a_{ij}(x_{\mathrm{r}j}(t) - x_{\mathrm{r}i}(t)) + k_i\Big(\theta_i(t) + \sum_{j\in N_i\setminus\mathcal{N}_{\mathrm{p}}} a_{ij}\big(x_j(t) - x_i(t)\big)\Big), \tag{9}$$

where $l_i \in \mathbb{R}_{>0}$ if $i \in \mathcal{N}_{\mathrm{p}'}$, $l_i = 0$ otherwise. Note that we utilize the reference consensus model (2) in the third protocol.

4 Fourth Protocol (LCP 4)

This protocol is mainly built on the second protocol with some modifications such as including the damping term used in the third protocol and removing the last summation in (6), which results in addressing *ii*) with no need of Assumption 2. Then, the fourth protocol is given by

$$u_i(t) = l_i(x_{\mathrm{r}i}(t) - x_i(t)) + \sum_{j\in N_i} a_{ij}(q_j(t) - q_i(t)) + k_i\theta_i(t), \tag{10}$$

where $l_i \in \mathbb{R}_{>0}$ if $i \in \mathcal{N}_{\mathrm{p}}$, $l_i = 0$ otherwise. Note that the reference consensus model (5) is used in the fourth protocol.

5 Fifth Protocol (LCP 5)

This protocol is obtained by removing the last summation in the third protocol and allowing all agents to use the damping term in (9). Lastly, there is no need of Assumption 2 in this protocol. Now, the fifth protocol is given by

$$u_i(t) \;=\; l_i(x_{\mathrm{r}i}(t) - x_i(t)) + \sum_{j\in N_i} a_{ij}(x_{\mathrm{r}j}(t) - x_{\mathrm{r}i}(t)) + k_i\theta_i(t), \tag{11}$$

where $l_i \in \mathbb{R}_{>0}$ for all $i \in \mathcal{N}$. Note that this protocol also uses the reference consensus model (2).

The concise summary of the theoretical results with respect to the protocols in [1] is given in Table 1. Note that $\bar{x}_{\mathrm{r}}$ and $\bar{q}$ denote the desired consensus value and the consensus value, respectively, in Table 1. They satisfy $\bar{x}_{\mathrm{r}} = w_l^{\mathrm{T}} x_{\mathrm{r}0}$ and $\bar{q} = w_l^{\mathrm{T}} q_0$, where $w_l^{\mathrm{T}} L = 0$ and $w_l^{\mathrm{T}} \mathbf{1}_N = 1$.

B Leader-Follower Consensus as a Global Objective

In order to obtain L-FCPs, LCPs presented in Section III-A are modified by using an extra term either $s_i(r - x_{\mathrm{r}i}(t))$ or $s_i(r - q_i(t))$. In particular, the former is added to (2), (4), (9), and (11) and the latter is added to (5), (6), and (10), which yield five L-FCPs; that is, LCP i becomes L-FCP i, where $i = 1, \ldots, 5$. We also note that if the information flows from the leader node v_0 to an agent v_i in V, then there exists an edge (v_0, v_i) with the weighting gain $s_i > 0$; otherwise $s_i = 0$. Define a matrix $S \triangleq \mathrm{diag}(s_1, \ldots, s_N)$. Based on this information, (2) and (5) can be rewritten as

$$\dot{x}_{\mathrm{r}i}(t) \;=\; \sum_{j\in N_i} a_{ij}(x_{\mathrm{r}j}(t) - x_{\mathrm{r}i}(t)) + s_i(r - x_{\mathrm{r}i}(t)), \quad x_{\mathrm{r}i}(0) = x_{\mathrm{r}i0}, \quad t \geq 0, \tag{12}$$

$$\dot{x}_{\mathrm{r}i}(t) \;=\; \sum_{j\in N_i} a_{ij}(q_j(t) - q_i(t)) + s_i(r - q_i(t)), \quad x_{\mathrm{r}i}(0) = x_{\mathrm{r}i0}, \quad t \geq 0, \tag{13}$$

respectively. Then, (12) can be compactly written as

$$\dot{x}_{\mathrm{r}}(t) = -(L + S)x_{\mathrm{r}}(t) + Sr_{\mathrm{a}}, \quad x_{\mathrm{r}}(0) = x_{\mathrm{r}0}, \quad t \geq 0, \tag{14}$$

Table 1. Summary of the theoretical results with respect to LCPs in [1].

Protocols	Assumptions	Conclusions
1	1,3	$\lim_{t\to\infty}(x_i(t)-\bar{x}_{\rm r})=0,\ \forall i\in\mathcal{N}_{\rm p'}$
	In addition, 2	For $i\in\mathcal{N}_{\rm p}$, $\lim_{t\to\infty}(x_i(t)-\bar{x}_{\rm r})=\begin{cases}0 & \text{if } \lim_{t\to\infty}\theta_i(t)=0\\ (1/d_{{\rm p}i})\theta_i^\star & \text{if } \lim_{t\to\infty}\theta_i(t)=\theta_i^\star\ (\theta_i^\star \text{ is finite})\end{cases}$
2	1	$\lim_{t\to\infty}(x_i(t)-\bar{q})=0,\ \forall i\in\mathcal{N}_{\rm p'}$
	In addition, 2	For $i\in\mathcal{N}_{\rm p}$, $\lim_{t\to\infty}(x_i(t)-\bar{q})=\begin{cases}0 & \text{if } \lim_{t\to\infty}\theta_i(t)=0\\ (1/d_{{\rm p}i})\theta_i^\star & \text{if } \lim_{t\to\infty}\theta_i(t)=\theta_i^\star\end{cases}$
3	1	$\lim_{t\to\infty}(x_i(t)-\bar{x}_{\rm r})=0,\ \forall i\in\mathcal{N}_{\rm p'}$
	In addition, 2	For $i\in\mathcal{N}_{\rm p}$, $\lim_{t\to\infty}(x_i(t)-\bar{x}_{\rm r})=\begin{cases}0 & \text{if } \lim_{t\to\infty}\theta_i(t)=0\\ (1/d_{{\rm p}i})\theta_i^\star & \text{if } \lim_{t\to\infty}\theta_i(t)=\theta_i^\star\end{cases}$
4	1	$\lim_{t\to\infty}(x_i(t)-\bar{q})=0,\ \forall i\in\mathcal{N}_{\rm p'}$
		For $i\in\mathcal{N}_{\rm p}$, $\lim_{t\to\infty}(x_i(t)-\bar{q})=\begin{cases}0 & \text{if } \lim_{t\to\infty}\theta_i(t)=0\\ (k_i/l_i)\theta_i^\star & \text{if } \lim_{t\to\infty}\theta_i(t)=\theta_i^\star\end{cases}$
5	1	$\lim_{t\to\infty}(x_i(t)-\bar{x}_{\rm r})=0,\ \forall i\in\mathcal{N}_{\rm p'}$
		For $i\in\mathcal{N}_{\rm p}$, $\lim_{t\to\infty}(x_i(t)-\bar{x}_{\rm r})=\begin{cases}0 & \text{if } \lim_{t\to\infty}\theta_i(t)=0\\ (k_i/l_i)\theta_i^\star & \text{if } \lim_{t\to\infty}\theta_i(t)=\theta_i^\star\end{cases}$

where $r_{\rm a}\triangleq r\mathbf{1}_N$. By using (13) and (1) with L-FCPs 2 or 4, we obtain

$$\dot{q}(t)=-(L+S)q(t)+Sr_{\rm a},\quad q(0)=q_0,\quad t\geq 0. \tag{15}$$

Note that $-(L+S)$ is Hurwitz under Assumption 4 [Lemma 3.3, 4].

Remark 2. If Assumption 1 and both $\bar{x}_{\rm r}$ and $\bar{q}$ in Table 1 are replaced with Assumption 4 and r, respectively, then all results in Table 1 hold for L-FCPs. In particular, $\lim_{t\to\infty}x_{{\rm r}i}(t)=r,\ \forall i\in\mathcal{N}$ for L-FCPs 1, 3, and 5, and $\lim_{t\to\infty}x_{{\rm r}i}(t)=r,\ \forall i\in\mathcal{N}_{\rm p}$ and $\lim_{t\to\infty}x_i(t)=r,\ \forall i\in\mathcal{N}_{\rm p'}$ for L-FCPs 2 and 4 under Assumption 4 by [Theorem 3.1, 5]. With the slight modification of the protocols given in Section III-A, the error dynamics in [1] does not change. Hence, the results hold. One can also show that if $r(t)$ is a time-varying signal and $\dot{r}(t)$ is a piecewise continuous signal that is converging to zero, then the results given in the Table 1 hold for L-FCPs when we replace $\bar{x}_{\rm r}$ and $\bar{q}$ with $r(t)$.

IV Experimental Setup

In this section, we provide specifications of the platforms used in this paper, and local and global objectives of the multiagent system together with its system parameters. The experiment is implemented in a pseudo-

distributed manner, where a workstation computer plays the critical role as a node for collecting data and calculating the distributed control signals before sending them to the robots for execution. We note here that the data is governed in such a way that each robot can have access only to some of its neighbors' information during the process of generating control signals.

A Khepera IV

Khepera IV ground mobile robot in [6] will be used as the experimental platform in this paper. The robot has the ability to operate autonomously for more than 5 hours with motors at full power [7]. In addition, this differential drive robot is equipped with various sensors including infrared sensors, ultrasonic sensors, camera, accelerometer, and gyroscope. Furthermore, Khepera IV robot has Gumstix Overo processor board allowing Bluetooth and WiFi communication. The Gumstix Overo comes with a Linux system and a built-in Bluetooth server for remote control purpose. In particular, the Bluetooth server enables the robot to receive commands from the workstation for execution and send the responses back. Since the Bluetooth communication on the robot may not be reliable, we use WiFi communication over the User Datagram Protocol (UDP). In particular, to take advantages of the built-in Bluetooth server, the robot is set up to listen to a UDP port for commands; once the commands are received, they will be forwarded to the Bluetooth server for execution and getting responses. After collecting the responses, the robot will send them back to the earlier sender, which is the workstation.

B Motion Capture System

The motion capture system (MoCap system) being used in this experiment consists of 5 Vicon Vero 2.2 cameras in [8] to cover the workspace of the robots. Specifically, the system can process up to 330 fps with a camera latency of 3.6 ms [8]. The system has ability to recognize and track photosensitive markers. To this end, the tracker software in [9] is used to collect and process data from cameras. In particular, a set of markers are mounted on top of each robot, then the tracker software allows the user to define this set as an object for tracking. A specific point relative to the markers can be chosen as the robot position. The position of each robot can also be accessed from MATLAB, which is used to generate control signals for the robots.

C Local and Global Objectives

For our experiments, we utilize six Khepera IV ground mobile robots to make the certain robots (i.e., agents) do local tasks and all agents do a global task (i.e., either the leaderless consensus or the leader-follower consensus) with respect to the graph topologies given in Figure 2. The local tasks are only assigned to agents 2 and 4. Thus, $\mathcal{N}_{\mathrm{p}} = \{v_2, v_4\}$ and $\mathcal{N}_{\mathrm{p}'} = \{v_1, v_3, v_5, v_6\}$. For experiments including a leader, only agent 3 is receiving the external reference signal from the leader. To accomplish local and global tasks, it is expected from the corresponding agents to move inside the desired regions illustrated in figures (see, for example, Figures 3 and 5). With respect to the desired region for the global task, we use a large square with a solid black line. For the local tasks, the desired regions are depicted by small squares having solid lines with three different colors. Specifically, we define the following rule for the agents subject to local tasks (i.e., agents 2 and 4). If there is a square with the same color representing either agent 2 or agent 4, it is expected from only that agent to move inside that square area, otherwise this agent(s) is expected to get inside the square with a different color than its own color. If a local task or a global task changes during the experiment, the previous task is kept by showing squares with dashed lines. Furthermore, the initial position of each agent in the experiments is denoted by "x" in Figures 3-18 except 13. It is also noted that we use the same desired regions in each experiment for the local and global tasks for LCPs and L-FCPs except the global task in L-FCPs.

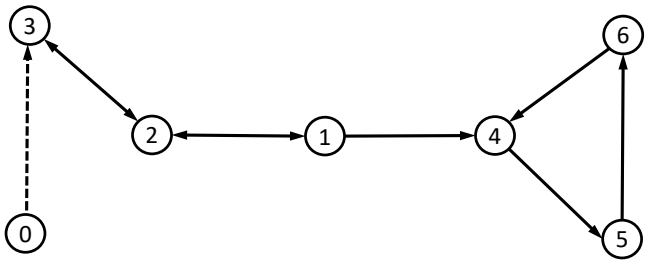

Figure 2. The graph topology $\mathcal{G}$ of the multiagent system composed of agents $v_1, \ldots, v_6$ and the augmented graph topology $\bar{\mathcal{G}}$ of the same system with the addition of the leader agent v_0.

D System Parameters and Initialization

The dynamics of each agent given in (1) is scalar. However, the ground mobile robots have a two-dimensional setting. Hence, the protocols given in Section III are applied as is to two dimensions (i.e., x and y axes).

In the experiments, we realized that the system dynamics (1) does not match the response of each ground mobile robot. Therefore, after a few trial and error processes on robots, we regard the model of each robot as

$$\dot{x}_i(t) \quad = \quad \gamma u_i(t), \quad x_i(0) = x_{i0}, \quad t \geq 0, \tag{16}$$

where $\gamma = 0.1$. As a result of this, the right hand sides of (2), (5), (12), and (13) are multiplied by γ as well. This alteration does not change the results given in Table 1 for LCPs and its L-FCPs counterpart. Moreover, if the following parameters are nonzero, we set $a_{ij} = 1$, $k_i = 1$, $l_i = 2$, and $s_i = 1$. Except s_i, they are specifically assigned in order to make the system matrix, which is scalar, of error dynamics (25), (27), (28), (29), and (19) given in [1] consistent. Otherwise, this causes different transient performances of the multiagent system for protocols used in the experiments.

With respect to the initialization, we set the actual initial position of each agent in x and y axes for LCPs 2-5 as follows: $x(0) = [-60, -100, -60, -100, -140, -140]^{\mathrm{T}}$ cm and $y(0) = [120, 80, -120, -80, 35, -35]^{\mathrm{T}}$ cm. The desired consensus value, which is 40 cm in x axis and 0 cm in y axis, for LCPs refers to the center of the desired region of the global task. Note that LCPs 2 and 4 may not provide a flexibility to choose the consensus value $\bar{q}$ as desired without modifying the actual initial position of some agents. However, we obtain $w_l = [1/3, 1/3, 1/3, 0, 0, 0]^{\mathrm{T}}$ for the graph topology $\mathcal{G}$ given in Figure 2, which satisfies $w_l^{\mathrm{T}} L = 0$ and $w_l^{\mathrm{T}} \mathbf{1}_N = 1$. Since $q(0) = [x_1(0), x_{\mathrm{r}2}(0), x_3(0), x_{\mathrm{r}4}(0), x_5(0), x_6(0)]^{\mathrm{T}}$ in x axis, the corresponding values of $x_{\mathrm{r}2}(0)$ and $x_{\mathrm{r}4}(0)$ in w_l are nonzero and zero, respectively, we can obtain $\bar{q}$ as desired by judiciously picking only $x_{\mathrm{r}2}(0)$. Therefore, the following reference initial values $x_{\mathrm{r}2}(0) = 240$ cm and $y_{\mathrm{r}2}(0) = 0$ cm are selected for agent 2 in these protocols. We also randomly set $x_{\mathrm{r}4}(0) = -120$ cm and $y_{\mathrm{r}4}(0) = -60$ cm. For the third and fifth protocols of LCPs, we set the reference initial states of the agents as follows: $x_{\mathrm{r}}(0) = [-60, 240, -60, -120, -140, -140]^{\mathrm{T}}$ cm and $y_{\mathrm{r}}(0) = [120, 0, -120, -60, 35, -35]^{\mathrm{T}}$ cm to drive all agents to the desired region of the global task. The following actual initial conditions $x(0) = [60, -20, 80, -100, -60, -100]^{\mathrm{T}}$ cm and $y(0) = [90, 0, -90, -120, -80, 100]^{\mathrm{T}}$ cm are set for experiments where LCP 1 and the standard consensus algorithm are implemented for the same purpose mentioned above. Due to Assumption 3, the reference and actual initial conditions of the agents are selected as the same value. We also note that the reference and actual initial conditions given above for LCPs are used in L-FCPs as well.

In terms of the desired regions for the local tasks in the experiments, we utilize $\theta_{xi}(t)$ and $\theta_{yi}(t)$ in x and y axes, respectively. In order to show the way we arrange the desired regions for all local tasks, we present

the calculation of the desired region for the local task of agent 2 until 100 sec. For this case, we regard -40 cm in x axis and 75 cm in y axis, which is in the desired region for the local task of agent 2 as shown in the first subfigure of Figure 3, as the desired steady state value of agent 2. Since the steady state value of agent 2 is $\bar{x}_{\mathrm{r}} + (1/d_{\mathrm{p}2})\theta_{x2}$ in x axis as given in Table 1, the desired consensus value is 40 cm (i.e., $\bar{x}_{\mathrm{r}}$) in x axis as given above, and $(1/d_{\mathrm{p}2}) = 1/2$, θ_{x2} is determined to be -160 cm. Similarly, the steady state value of agent 2 is $\bar{y}_{\mathrm{r}} + (1/d_{\mathrm{p}2})\theta_{y2}$ in y axis, where $\bar{y}_{\mathrm{r}} = 0$ cm and $(1/d_{\mathrm{p}2}) = 1/2$. Then, we can obtain $\theta_{y2} = 150$ cm.

V Experimental Results

In this section, we present the experimental results of implementing the protocols given in Section III with the setup in Section IV on a team of ground mobile robots shown in Figure 1 to compare their performances. This section is divided into two parts: Leaderless consensus as a global objective and leader-follower consensus as a global objective. Note that the graph topologies given in Figure 2 satisfy Assumptions 1 and 4 for LCPs and L-FCPs, respectively. Based on the information in Section IV-C, Assumption 2 also holds in our experiments.

A Leaderless Consensus as a Global Objective

1 First Protocol (LCP 1)

The experimental result of LCP 1 is given in Figure 3. It shows that all tasks are accomplished except that agent 6 reaches the desired region in 130 sec.

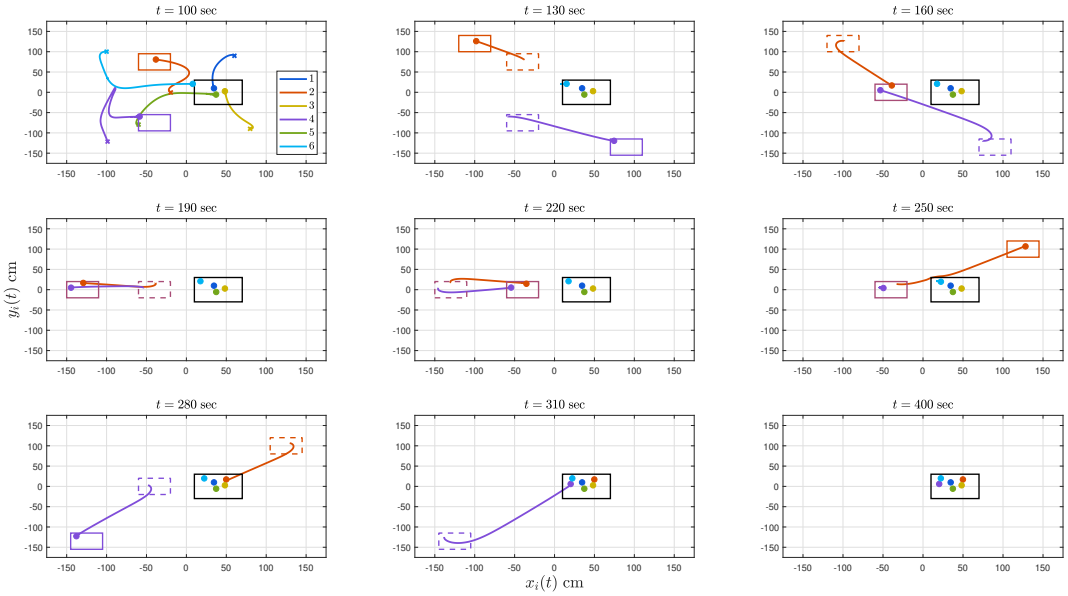

Figure 3. The response of each agent with LCP 1, where "x" denotes the actual initial position of each agent in the first subfigure; the solid lines denote the trajectory of each agent; the circles denote the position of each agent at the time specified on the top of each subfigure; the square box with solid black line denotes the desired region for the global objective; other square boxes with different solid color lines denote the desired region for the local objectives; the square boxes with dashed lines denote the previous desired regions.

In addition, we examine this protocol in terms of its robustness to the parameter γ (i.e., modeling error). First, γ is increased from 0.1 to 1, which would be the case if γ was not determined in Section IV-D. As it can be observed in Figure 4 (a) that the agents do not complete their tasks. That is because, the new reference model of each agent does not match its actual dynamics. Specifically, since γ is increased, the Fiedler eigenvalue of the resulting graph Laplacian becomes larger; hence, the reference models of the multiagent

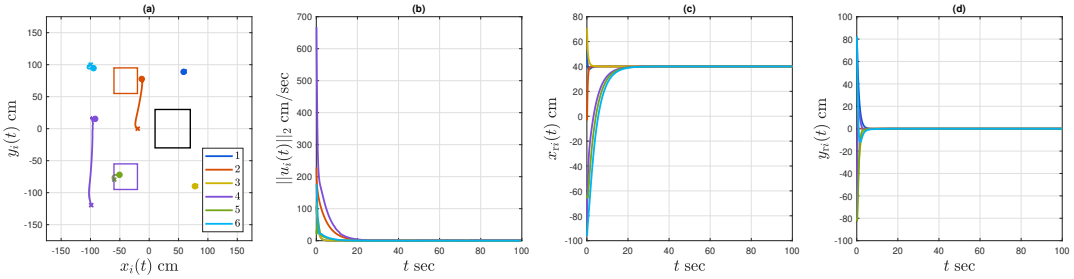

Figure 4. Figure (a) shows the response of each agent until 100 sec with LCP 1, where "x" denotes the actual initial position of each agent; the solid lines denote the trajectory of each agent; the circles denote the position of each agent at 100 sec; the square box with solid black line denotes the desired region for the global objective; other square boxes with different solid color lines denote the desired regions for the local objectives. Figure (b) shows the Euclidean norm of the control input applied to each agent. Figure (c) and (d) show the reference state of each agent.

system reaches the consensus with a smaller time constant (see Figures 4 (c) and (d)). In conjunction with (4), this explains why $u_i(t)$ approaches zero within 20 sec for all $i \in \mathcal{N}_{\mathrm{p}'}$ (see Figure 4 (b)). Thus, the robots in $\mathcal{N}_{\mathrm{p}'}$ do not even move after 20 sec. Since these agents do not complete their global task, agents 2 and 4 do not accomplish their local tasks either. Second, γ is decreased from 0.1 to 0.03. It is observed that although the control input of each agent does not approach zero as fast as the previous experiment, the agents still do not accomplish their tasks. We infer from these three experiments that the modeling error plays an important role in the accomplishment of the tasks when LCP 1 is implemented.

2 Second and Fourth Protocols (LCPs 2 and 4)

Now, we investigate the experimental results of LCPs 2 and 4 in this subsection together since the responses of the multiagent system with these protocols show similarities. It is seen from Figures 5 and 6 that the agents fail to perform their global task eventually although they do their local and global tasks until 310 sec with some imperfections. Since the system matrix in (8) is not Hurwitz, under an external input the resulting system is not input-to-state stable. Therefore, a simple disturbance may cause the drift from the desired region as shown in the last subfigures of Figures 5 and 6. To see whether this is the reason behind this drift, we also implement the standard consensus protocol (i.e., $u_i(t) = \sum_{j \in N_i} a_{ij}(x_j(t) - x_i(t))$), which yields a non-Hurwitz system matrix as in (8), in the experiment. Figure 7 shows that the agents move in the desired region and they do not move away from there as opposed to LCPs 2 and 4.

Furthermore, we examine the effect of the reference models in LCPs 2 and 4 on the response of the multiagent system. Notice that LCP 4 does not have any restriction on selecting agents for local tasks, compared to LCP 2, which relies on Assumption 2. Owing to this convenience, we utilize LCP 4 in the following experiments: Agents 1 and 3 are assigned the local tasks in addition to agents 2 and 4. During the whole experiment, it is expected that the former agents only move in the desired region for the global task in contrast to the latter agents sent to the desired regions for the local tasks. Figure 8 illustrates a great improvement in the performances of the agents for accomplishing not only the local tasks but also the global task without the drift. On the other hand, when we assign the local tasks to agents 5 and 6 instead of agents 1 and 3 in the previous scenario, we observe that a drift occurs during the experiment as shown in Figure 9. Note that if we assign all agents to the local tasks, then LCP 4 is nothing but LCP 5 (see the response of LCP 5 in Figure 11). Therefore, not only the number of agents in $\mathcal{N}_{\mathrm{p}}$ but also their selection significantly affect the response of the multiagent system for LCP 4.

Based on these observations, there is unlikely an external disturbance perturbing the system in such a way that the agents move away from the desired region. On the contrary, the problem arises from the information exchange between the reference states of agents $i \in \mathcal{N}_{\mathrm{p}}$ and the actual states of agents $i \in \mathcal{N}_{\mathrm{p}'}$ in LCPs 2 and 4. That is because, the reference model of each agent does not take the physical constraints into account such as the physical interactions among robots and the diameters of robots occupying the exact desired point, which is the center of the desired region.

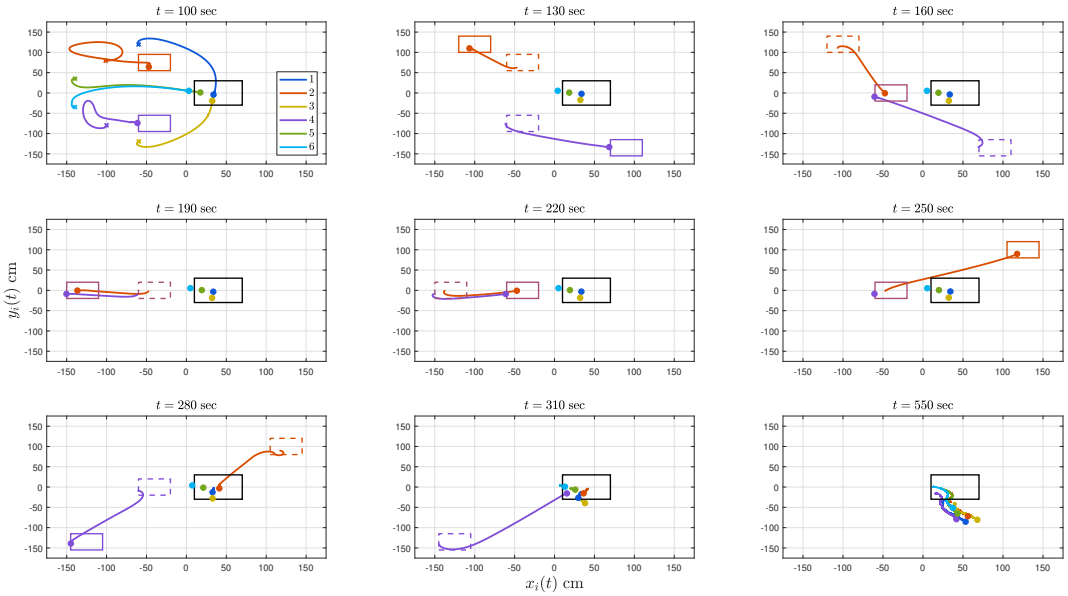

Figure 5. The response of each agent with LCP 2, where "x" denotes the actual initial position of each agent in the first subfigure; the solid lines denote the trajectory of each agent; the circles denote the position of each agent at the time specified on the top of each subfigure; the square box with solid black line denotes the desired region for the global objective; other square boxes with different solid color lines denote the desired region for the local objectives; the square boxes with dashed lines denote the previous desired regions.

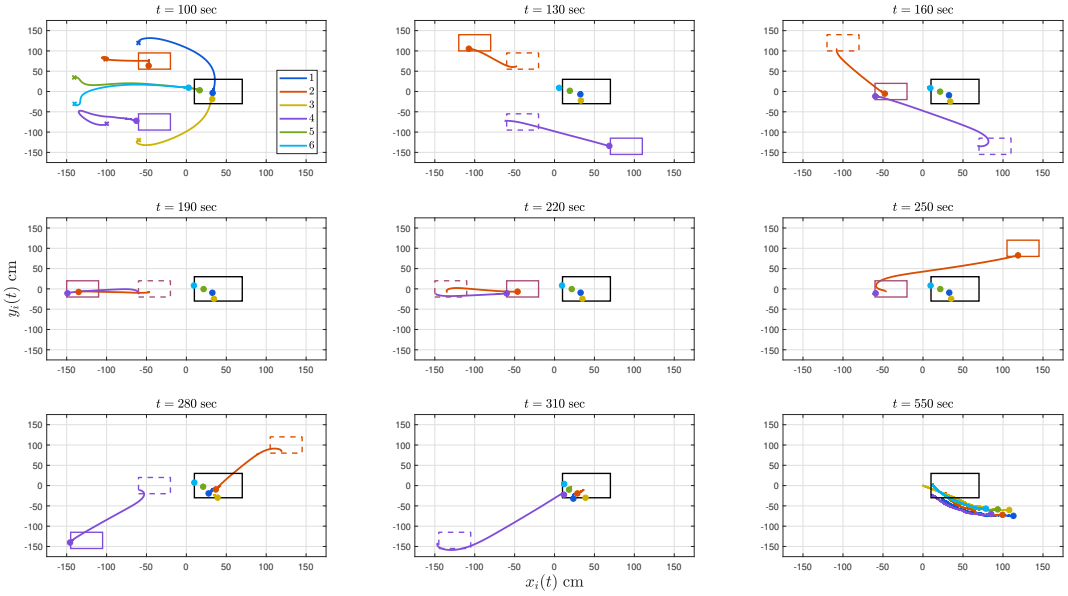

Figure 6. The response of each agent with LCP 4, where "x" denotes the actual initial position of each agent in the first subfigure; the solid lines denote the trajectory of each agent; the circles denote the position of each agent at the time specified on the top of each subfigure; the square box with solid black line denotes the desired region for the global objective; other square boxes with different solid color lines denote the desired region for the local objectives; the square boxes with dashed lines denote the previous desired regions.

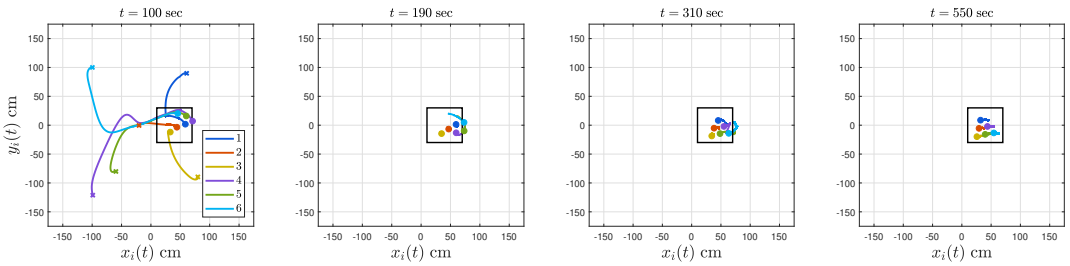

Figure 7. The response of each agent with the standard consensus protocol, where "x" denotes the actual initial position of each agent in the first subfigure; the solid lines denote the trajectory of each agent; the circles denote the position of each agent at the time specified on the top of each subfigure; the square box with solid black line denotes the desired region for the consensus.

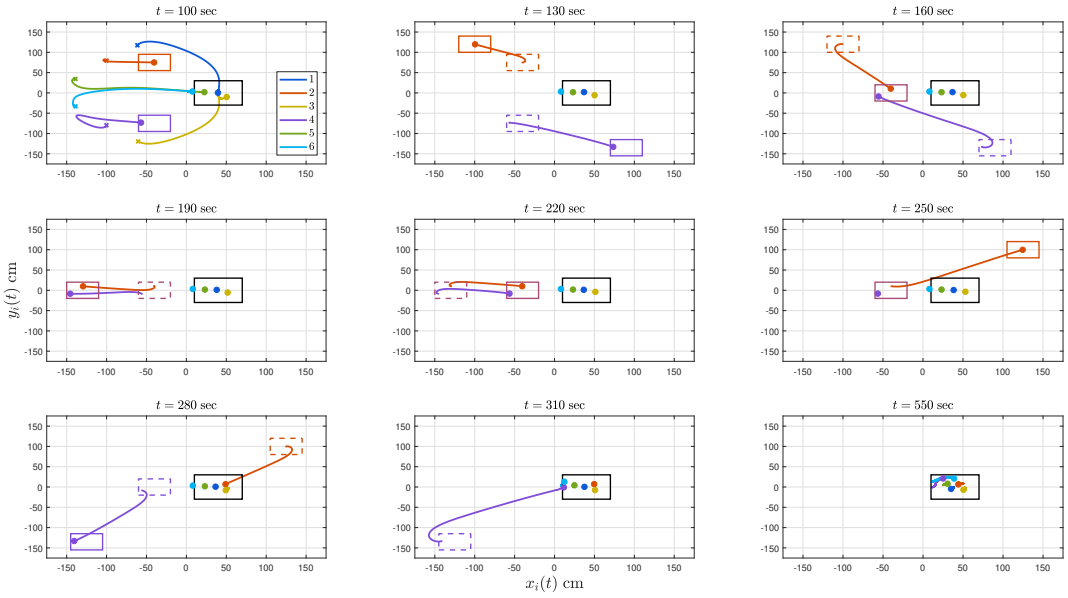

Figure 8. The response of each agent with LCP 4, where "x" denotes the actual initial position of each agent in the first subfigure; the solid lines denote the trajectory of each agent; the circles denote the position of each agent at the time specified on the top of each subfigure; the square box with solid black line denotes the desired region for the global objective; other square boxes with different solid color lines denote the desired region for the local objectives; the square boxes with dashed lines denote the previous desired regions.

3 Third and Fifth Protocols (LCPs 3 and 5)

Similar to the previous subsection, we investigate the experimental results of LCPs 3 and 5 in this subsection together. It is clear that all agents accomplish their tasks with these protocols as shown in Figures 10 and 11. In contrast to LCPs 2 and 4, the agents keep still after they move in the desired region for the global task.

To see the robustness of these protocols to the parameter γ, we first increase γ from 0.1 to 1. From Figures 12 and 13, it is evident that the agents accomplish their tasks and the multiagent system has a faster response, respectively. Specifically, the agents settle to the desired values around 30 sec in Figure 13 but it takes around 90 sec when $\gamma = 0.1$. We then decrease γ from 0.1 to 0.03 and repeat the experiment, the agents accomplish their tasks relatively slower. As a conclusion of these two experiments, we may adjust the speed of the completion for tasks by modifying γ.

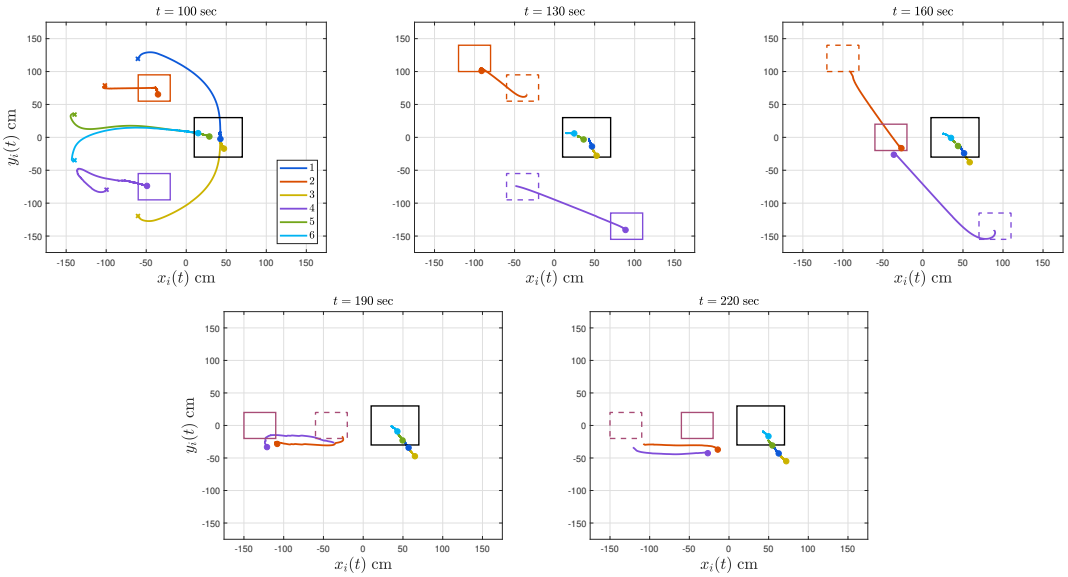

Figure 9. The response of each agent with LCP 4, where "x" denotes the actual initial position of each agent in the first subfigure; the solid lines denote the trajectory of each agent; the circles denote the position of each agent at the time specified on the top of each subfigure; the square box with solid black line denotes the desired region for the global objective; other square boxes with different solid color lines denote the desired region for the local objectives; the square boxes with dashed lines denote the previous desired regions.

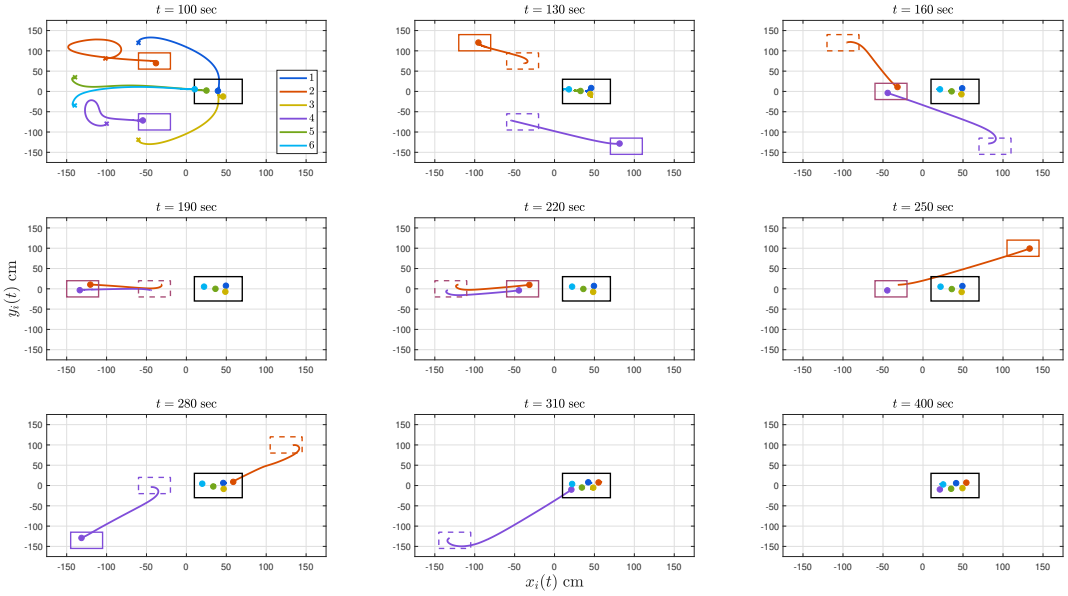

Figure 10. The response of each agent with LCP 3, where "x" denotes the actual initial position of each agent in the first subfigure; the solid lines denote the trajectory of each agent; the circles denote the position of each agent at the time specified on the top of each subfigure; the square box with solid black line denotes the desired region for the global objective; other square boxes with different solid color lines denote the desired region for the local objectives; the square boxes with dashed lines denote the previous desired region.

B Leader-Follower Consensus as a Global Objective

In this part, we additionally consider $r_x(t)$ and $r_y(t)$ in the experiments, which denote the external reference signals in x and y axes, respectively. These signals are given by

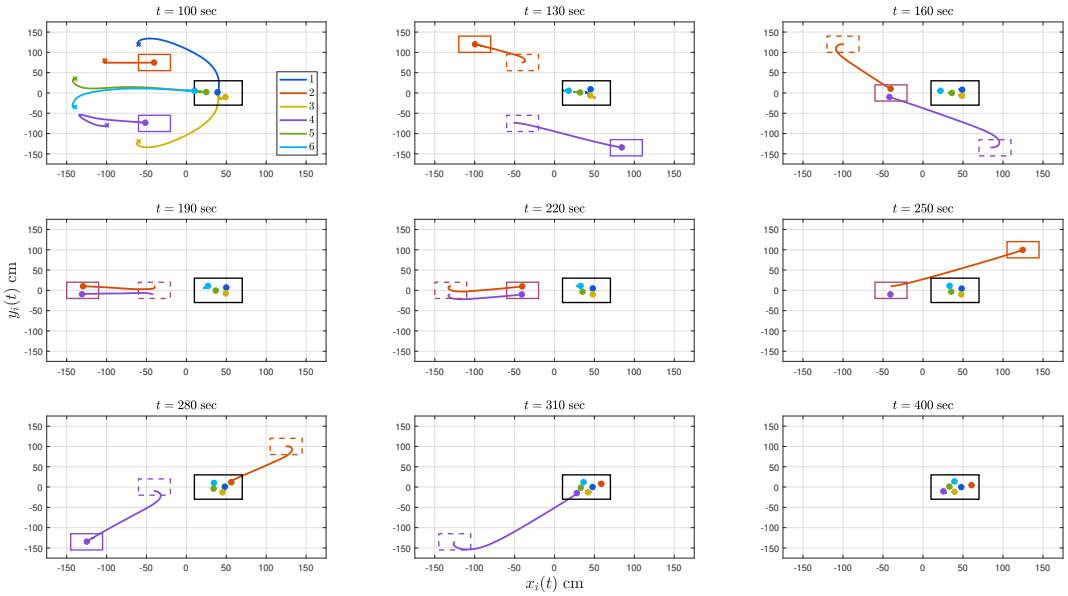

Figure 11. The response of each agent with LCP 5, where "x" denotes the actual initial position of each agent in the first subfigure; the solid lines denote the trajectory of each agent; the circles denote the position of each agent at the time specified on the top of each subfigure; the square box with solid black line denotes the desired region for the global objective; other square boxes with different solid color lines denote the desired region for the local objectives; the square boxes with dashed lines denote the previous desired regions.

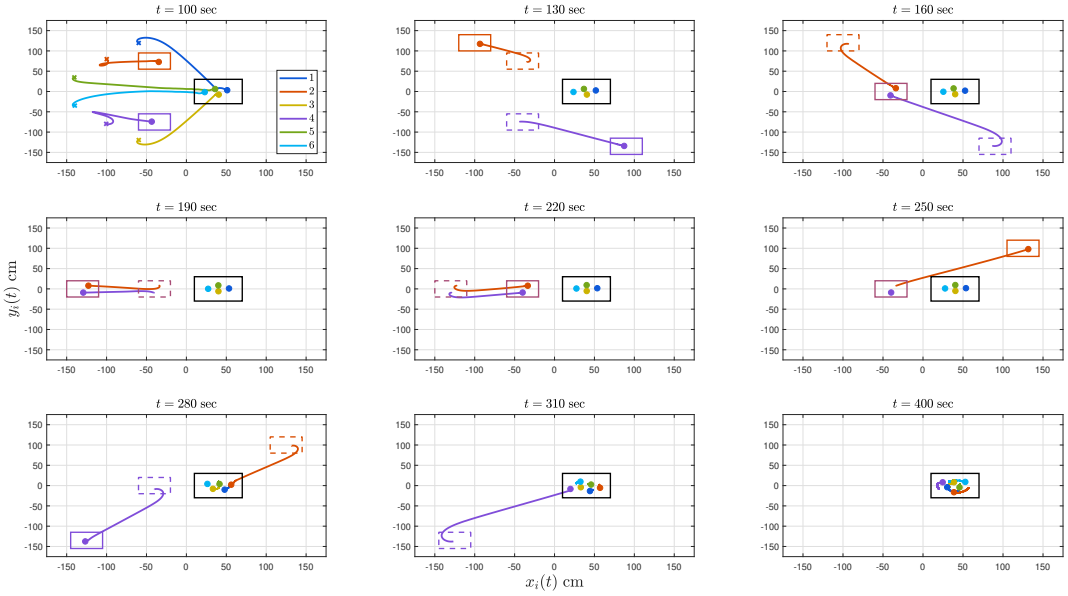

Figure 12. The response of each agent with LCP 3, where "x" denotes the actual initial position of each agent in the first subfigure; the solid lines denote the trajectory of each agent; the circles denote the position of each agent at the time specified on the top of each subfigure; the square box with solid black line denotes the desired region for the global objective; other square boxes with different solid color lines denote the desired region for the local objectives; the square boxes with dashed lines denote the previous desired regions.

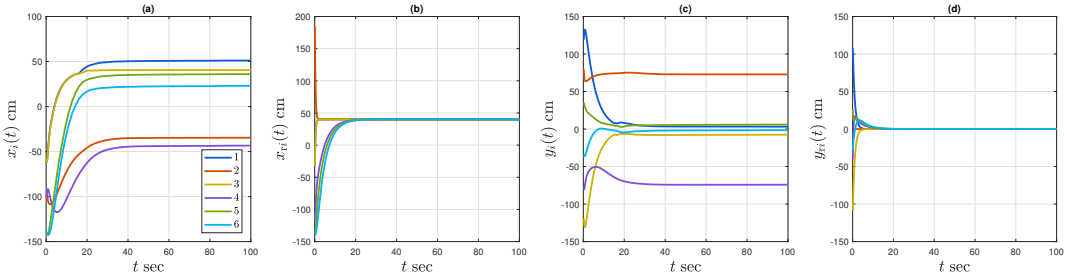

Figure 13. The response of each agent until 100 sec with LCP 3 is given in Figures (a)-(d). Figures (a) and (c) show the actual states of each agent in x and y axes, respectively. Figure (b) and (d) show the reference states of each agent in x and y axes, respectively.

$$r_x(t) = \begin{cases} 40 \text{ cm} & \text{if } t < 160 \text{ sec}, \\ 100 - 60e^{-0.02(t-160)} \text{ cm} & \text{if } t \geq 160 \text{ sec}, \end{cases}$$

$$r_y(t) = \begin{cases} 0 \text{ cm} & \text{if } t < 160 \text{ sec}, \\ -100 + 100e^{-0.02(t-160)} \text{ cm} & \text{if } t \geq 160 \text{ sec}. \end{cases}$$

Thus, it is expected from the agents to move in the last black box with the solid line around 400 sec.

Now, we present experimental results of L-FCPs. First, we discuss the experimental results of L-FCP 1. Figure 14 shows that the agents accomplish their local and global tasks except that agent 6 moves inside the desired region for the global task within 130 sec. Eventually, some agents cannot get in the desired region for the global task. It may be due to the fact that the robots are subject to the physical interaction with other robots during the movement toward another desired region after 160 sec. Second, we investigate the experimental results of L-FCPs 2 and 4. Figures 15 and 16 demonstrate that the agents do their local and global tasks until 310 sec with some imperfections. After 310 sec, the agents move away from the desired region for the global task as shown in these figures even though (8) becomes (15) with L-FCPs 2 and 4, in which the system matrix is Hurwitz; hence, the system is input-to-state stable. This also supports the conclusion drawn for LCPs 2 and 4. Third, we present the experimental results of L-FCPs 3 and 5. All agents accomplish their tasks with these protocols as shown in Figures 17 and 18.

VI Conclusions

This paper presented experimental evaluation of LCPs given in [1] and L-FCPs applied to a team of ground mobile robots. Experimental results revealed that the third and fifth protocols of LCPs and L-FCPs outperforms other protocols. Specifically, LCP 1 and L-FCP 1 accomplish the local and global tasks unless there are modeling errors. The structure of the second and fourth protocols of LCPs and L-FCPs lead the agents to a drift from the desired regions even though the agents do the local and global tasks with some imperfections until certain time. The third and fifth protocols of LCPs and L-FCPs do their tasks successfully even with an incorrect parameter γ in the refence model of each agent. Future research can include the improvement of the second and fourth protocols of LCPs and L-FCPs in order to eliminate the drift in the experiments.

VII Acknowledgments

This research was supported by the Republic of Turkey Ministry of National Education and the Dynamics, Control, and Systems Diagnostics Program of the National Science Foundation under Grant CMMI-1657637.

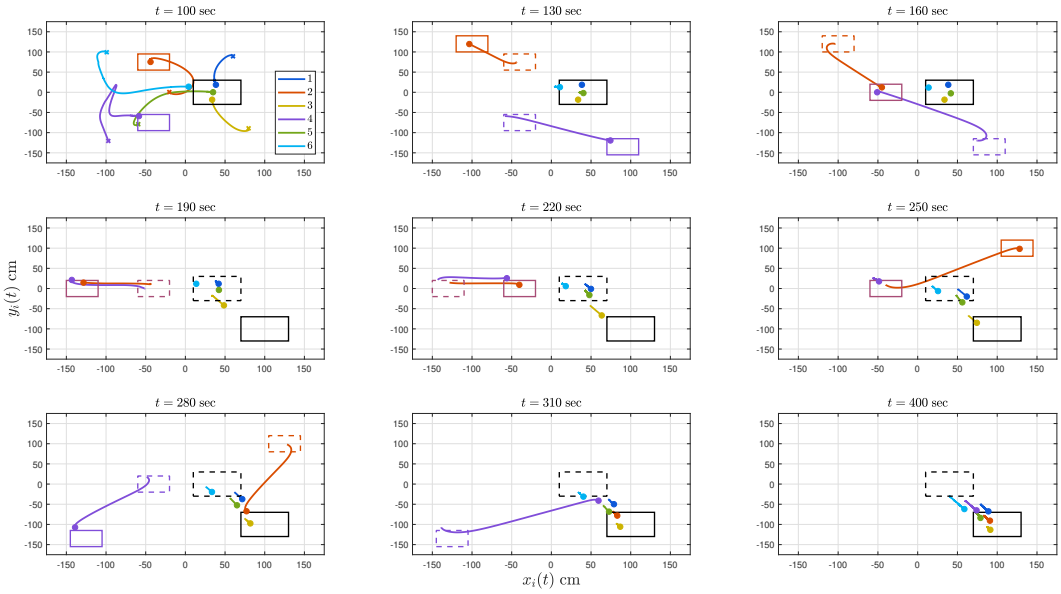

Figure 14. The response of each agent with L-FCP 1, where "x" denotes the actual initial position of each agent in the first subfigure; the solid lines denote the trajectory of each agent; the circles denote the position of each agent at the time specified on the top of each subfigure; the square box with solid black line denotes the desired region for the global objective; other square boxes with different solid color lines denote the desired region for the local objectives; the square boxes with dashed lines denote the previous desired regions. Note that it is expected from the agents to move in the last black box with the solid line around 400 sec.

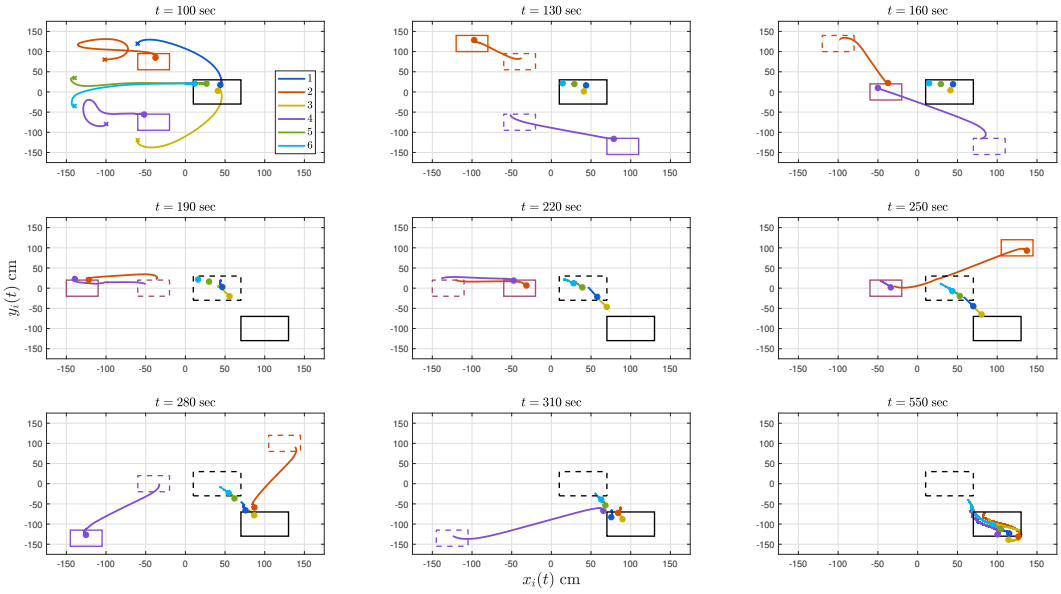

Figure 15. The response of each agent with L-FCP 2, where "x" denotes the actual initial position of each agent in the first subfigure; the solid lines denote the trajectory of each agent; the circles denote the position of each agent at the time specified on the top of each subfigure; the square box with solid black line denotes the desired region for the global objective; other square boxes with different solid color lines denote the desired region for the local objectives; the square boxes with dashed lines denote the previous desired regions. Note that it is expected from the agents to move in the last black box with the solid line around 400 sec.

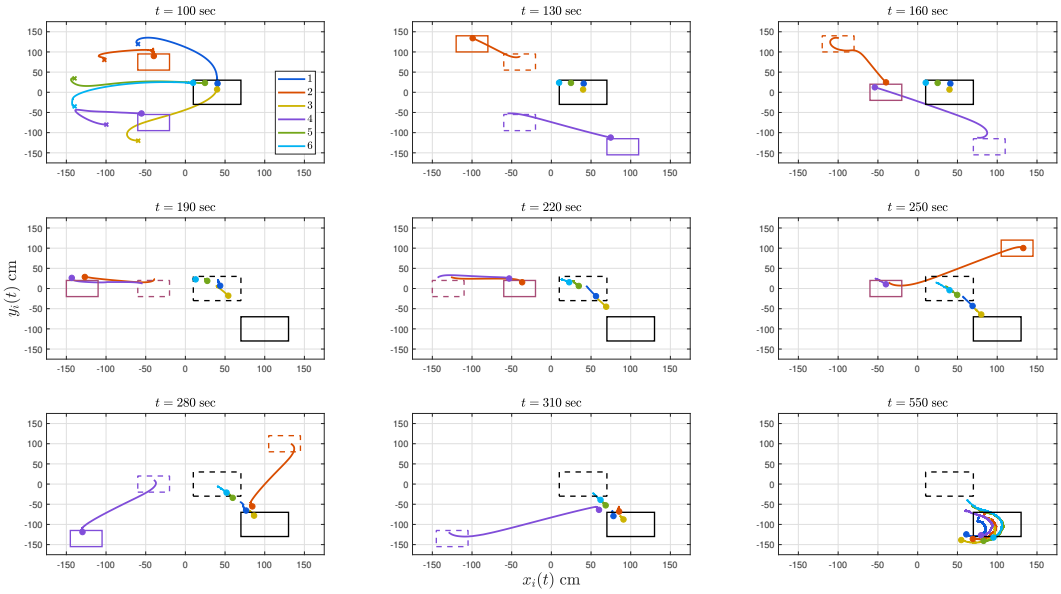

Figure 16. The response of each agent with L-FCP 4, where "x" denotes the actual initial position of each agent in the first subfigure; the solid lines denote the trajectory of each agent; the circles denote the position of each agent at the time specified on the top of each subfigure; the square box with solid black line denotes the desired region for the global objective; other square boxes with different solid color lines denote the desired region for the local objectives; the square boxes with dashed lines denote the previous desired regions. Note that it is expected from the agents to move in the last black box with the solid line around 400 sec.

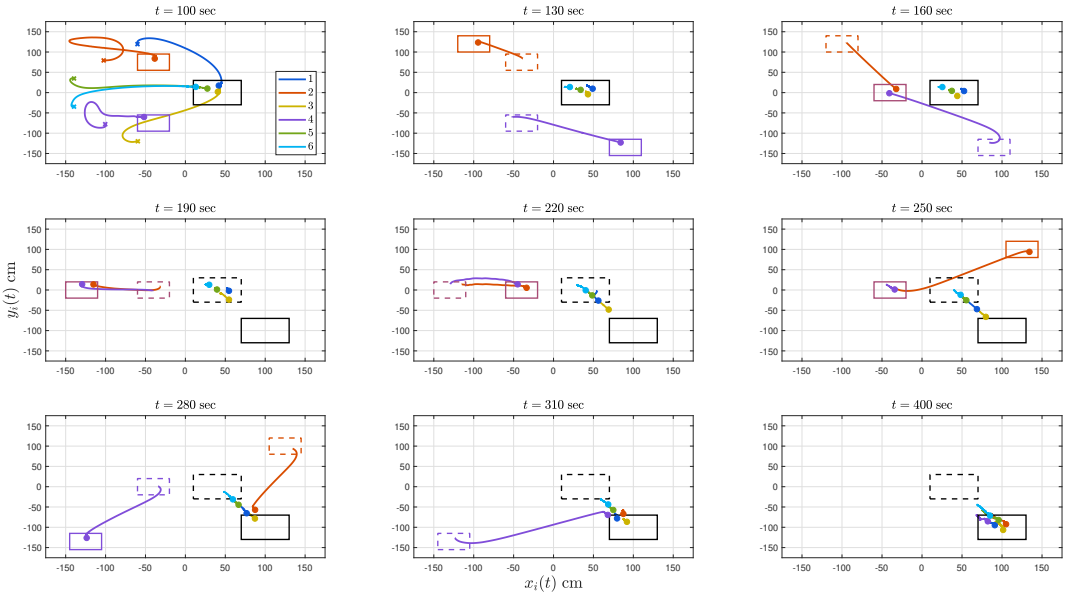

Figure 17. The response of each agent with L-FCP 3, where "x" denotes the actual initial position of each agent in the first subfigure; the solid lines denote the trajectory of each agent; the circles denote the position of each agent at the time specified on the top of each subfigure; the square box with solid black line denotes the desired region for the global objective; other square boxes with different solid color lines denote the desired region for the local objectives; the square boxes with dashed lines denote the previous desired regions. Note that it is expected from the agents to move in the last black box with the solid line around 400 sec.

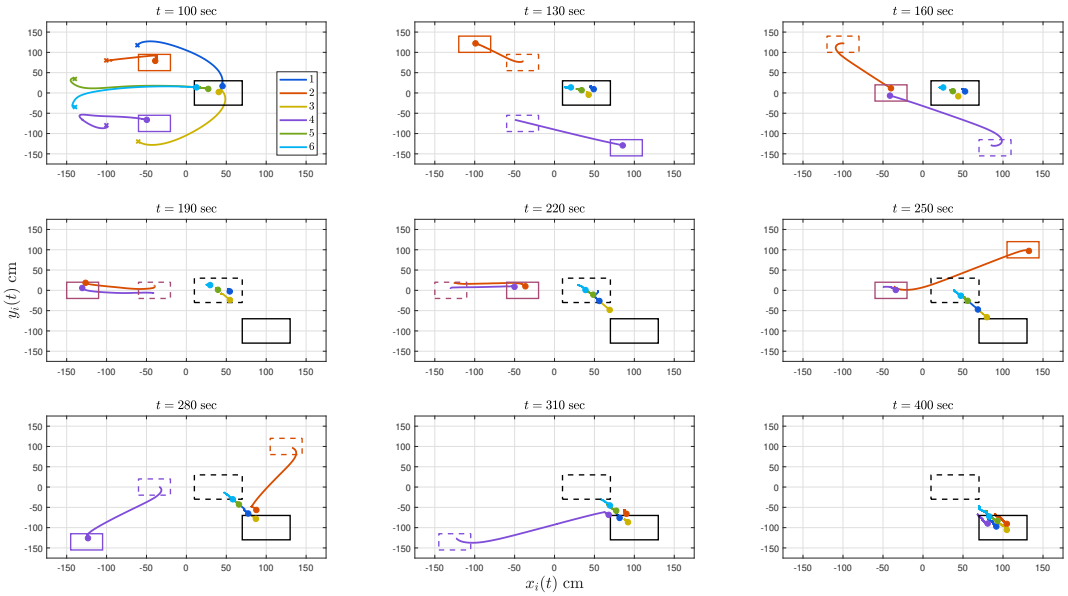

Figure 18. The response of each agent with L-FCP 5, where "x" denotes the actual initial position of each agent in the first subfigure; the solid lines denote the trajectory of each agent; the circles denote the position of each agent at the time specified on the top of each subfigure; the square box with solid black line denotes the desired region for the global objective; other square boxes with different solid color lines denote the desired region for the local objectives; the square boxes with dashed lines denote the previous desired regions. Note that it is expected from the agents to move in the last black box with the solid line around 400 sec.

References

[1]S. B. Sarsilmaz and T. Yucelen, "Control of multiagent systems with local and global objectives," in *IEEE Conference on Decision and Control*, 2018.

[2]R. Olfati-Saber and R. M. Murray, "Consensus problems in networks of agents with swtiching topology and time-delays," *IEEE Transactions on Automatic Control*, vol. 49, no. 9, pp. 1520–1533, 2004.

[3]M. Mesbahi and M. Egerstedt, *Graph theoretic methods in multiagent networks*. Princeton University Press, 2010.

[4]F. L. Lewis, H. Zhang, K. Hengster-Movric, and A. Das, *Cooperative control of multi-agent systems: Optimal and adaptive design approaches*. Springer, 2014.

[5]W. Ren, "Multi-vehicle consensus with a time-varying reference state," *Systems & Control Letters*, vol. 56, pp. 474–483, 2007.

[6]"Khepera IV," https://www.k-team.com/khepera-iv, [Accessed 30-May-2019].

[7]J. Tharin, F. Lambercy, and T. Carron, "Khepera iv user manual," *K-Team SA, Switzerland*, 2015.

[8]"Vicon vero," https://www.vicon.com/products/camera-systems/vero, [Accessed 30-May-2019].

[9]"Tracker," https://www.vicon.com/products/software/tracker, [Accessed 30-May-2019].